Semiconductor Science and Technology

Electrical and optical characterisation of low temperature grown InGaAs for photodiode applications

To cite this article before publication: Leh Woon Lim *et al* 2020 *Semicond. Sci. Technol.* in press https://doi.org/10.1088/1361-6641/aba167

IOP PublishingJournal Title
Journal **XX** (XXXX) XXXXXX https://doi.org/XXXX/XXXX

Electrical and optical characterisation of low temperature grown InGaAs for photodiode applications

Leh Woon Lim[1], Pallavi Patil[2], I. P. Marko[3], Edmund Clarke[2], S. J. Sweeney[3], Jo Shien Ng[1], John P R David[1], Chee Hing Tan[1]

[1] Department of Electronic and Electrical Engineering, University of Sheffield, Sheffield, S1 4DE, UK
[2] EPSRC National Epitaxy Facility, University of Sheffield, Sheffield, S3 7HQ, UK
[3] Advanced Technology Institute and Department of Physics, University of Surrey, Guildford, GU2 7XH, UK

E-mail: c.h.tan@sheffield.ac.uk

Received xxxxxx
Accepted for publication xxxxxx
Published xxxxxx

Abstract

Dilute bismide and nitride alloys are promising semiconductors for bandgap engineering, opening additional design freedom for devices such as infrared photodiodes. Low growth temperatures are required to incorporate bismuth or nitrogen into III-V semiconductors. However, the effects of low growth temperature on dark current and responsivity are not well understood. In this work, a set of InGaAs p-i-n wafers were grown at a constant temperature of 250, 300, 400 and 500 °C for all p, i and n layers. A second set of wafers was grown where the p and n layers were grown at 500 °C while the i-layers were grown at 250, 300 and 400 °C. Photodiodes were fabricated from all seven wafers. When constant growth temperature was employed (for all p, i and n layers), we observed that photodiodes grown at 500 °C show dark current density at -1 V that is 6 orders of magnitude lower while the responsivity at an illumination wavelength of 1520 nm is 4.5 times higher than those from photodiodes grown at 250 °C. Results from the second set of wafers suggest that performance degradation can be recovered by growing the p and n layers at high temperature. For instance, comparing photodiodes with i-layers grown at 250 °C, photodiodes showed dark current density at -1 V that is 5 orders of magnitude lower when the p and n layer were grown at 500 °C. Postgrowth annealing, at 595 °C for 15 minutes, on the two wafers grown at 250 and 300 °C showed recovery of diode responsivity but no significant improvement in the dark current. Our work suggests that growth of the cap layer at high temperature is necessary to maintain the responsivity and minimise the dark current degradation, offering a pathway to developing novel photodiode materials that necessitate low growth temperatures.

Keywords: Indium Gallium Arsenide, photodiodes, low temperature MBE growth

1. Introduction

Short-wave infrared (SWIR) imaging in the wavelength range of 1 to 3 μm is becoming a topic of great interest in applications such as remote sensing, night imaging, thermal imaging and free space optical communications [1]. Well-established III-V semiconductor detectors capable of SWIR detection include extended-wavelength InGaAs [2], InP-based type-II superlattice (T2SL) [3], GaSb-based T2SL [4] and InAs [5]. The most mature commercial option is the extended InGaAs. However, large lattice mismatch between extended-wavelength InGaAs (of high Indium composition) and InP

substrate gives rise to dislocations in the InGaAs crystal and non-ideal optoelectronic properties [6]. The superlattices offer bandgap tuning capability but are more difficult to grow due to complicated interfaces. InAs is a simple binary compound that can circumvent growth related issues in extended InGaAs and T2SL but has an inherently higher leakage current due to its narrower bandgap. In addition to III-V semiconductors, II-VI semiconductors such as PbS and HgCdTe (with appropriate Hg composition [7]) can also be operated in the SWIR wavelength range. The latter incurs high production costs and is incompatible with a global initiative to phase out mercury containing compounds from consumer products [8]. Therefore, having a SWIR detector material compatible with the InP platform, for example utilising dilute bismide [9,10], or nitride [11] incorporated into InGaAs, is attractive. This is due to their relatively low cost and mature processing but also in terms of compatibility to integrated InP photonics systems [12].

Nitrogen (N) [13] or Bismuth (Bi) [14] can be added to III-V compound semiconductors to induce a reduction in bandgap and consequently a longer cutoff wavelength. A significant bandgap reduction per percent of N is attainable [15], offering potentials as 1 eV bandgap material for GaAs-based multijunction solar cells [16] and photodiodes operating in the 1.3 µm telecommunications band [17]. Similarly, dilute Bi incorporation has been demonstrated in III-V semiconductors such as GaAs [18, 19], $In_{0.53}Ga_{0.47}As$ [20] (hereinafter referred to as InGaAs) and InAs [21].

The incorporation of N and Bi atoms requires epitaxial growth at temperatures lower than used for the conventional growth of generic GaAs or InGaAs alloys. Typically, growth temperatures between 375 to 500 °C [22-27] and 255 to 400 °C [28-31] has been used for dilute nitride and bismide alloys respectively. In comparison, conventional InGaAs growth via molecular beam epitaxy (MBE) is usually performed at temperatures above 500 °C [32,33]. It is, however, known that III-As semiconductors grown at low temperature suffer from loss of stoichiometry due to the incorporation of excess As [34,35]. As a result, increased carrier concentration and decreased mobility are commonly reported in low temperature grown InGaAs [36-38].

While there has been significant effort in growth and material characterization of $In_yGa_{1-y}As_{1-x}Bi_x$, the effects on dark current and responsivity brought upon by the low growth temperature is not well understood [39]. Similarly, a systematic investigation on the low temperature grown InGaAs devices using MBE has not yet been undertaken. This paper aims to provide insights into the influence of growth temperature on fundamental photodiode characteristics in InGaAs photodiodes with no Bi incorporation in preparation for future growth optimization for developing semiconductor materials grown at low temperature, such as Bi containing alloys.

2. Experimental details

A total of seven InGaAs wafers were grown on lattice matched n-type (001) InP substrates using MBE with growth temperatures ranging from 250 to 500 °C. For each wafer, a 500 nm n-type InGaAs layer was grown on the substrate followed by a 1000 nm undoped InGaAs layer and a 500 nm p-type InGaAs as the top cap layer. The growth rate used is 1.2 µm/hour and p and n layer doping concentrations are nominally 5×10^{18} cm^{-3}. Two sets of wafers (A and B) were grown. For a given wafer in set A, all layers were grown at the same temperature. In set B, the p and n layers were grown at 500 °C while the i-layer was grown at a lower temperature. Therefore the i-layers in set B wafers can be considered to have in-situ annealing when the p layer was grown at 500 °C. Table I summarises growth details for each wafer and the growth temperatures are calibrated with a kSA BandiT band-edge thermometry system with an uncertainty of ±10 °C.

To study the effects of postgrowth annealing on photodiode performance, ex-situ annealing on two samples from set A, A300-A and A250-A (annealing denoted by a '-A' suffix) were performed. A thin encapsulating layer of SiO_2 was deposited using plasma-enhanced chemical vapour deposition prior to annealing at 595 °C for 15 minutes in a nitrogen-rich environment using a rapid thermal annealer.

Standard photolithography process was used to fabricate mesa diodes of varying diameters (70 to 420 µm) from each wafer. Devices were etched with a 1:8:80 mixture of sulfuric acid (95%), hydrogen peroxide (30%) and de-ionised water. Ti/Au were deposited as the p and n-type contacts by thermal evaporation.

On wafer dark current-voltage (I-V) and capacitance-voltage (C-V) measurements were performed at room temperature using a picoammeter (HP Model 4140B) and an LCR meter (HP Model 4275A), respectively. Temperature dependent I-V measurements were performed using a Janis ST-500 cryogenic probe station. For I-V measurements, devices with diameters of 70, 120, 220 and 420 µm were characterised. Responsivity measurements at room temperature were performed by illuminating the top of mesa diodes of 420 µm diameter with 1520 nm wavelength light from a He-Ne laser. The resultant photocurrent was measured with a lock-in amplifier (Stanford Research Systems Model SR830) by a phase sensitive detection method. For electroluminescence (EL) measurements, mesa diodes of 420 µm diameter were wire bonded on 3 mm TO headers. A Keithley 2400 source-meter unit was used for continuous wave characterization and the EL spectra were collected using a 400 µm diameter core multimode optical fibre and a NIRQUEST-512-1.9 Ocean Optics spectrometer operating in 1100-1900 nm spectral range.

Table I Wafer details and key photodiode parameters presented in Fig. 2 and 3(a)

Wafer	i-layer growth temperature (°C)	p/n-layer growth temperature (°C)	Dark current density at -1 V bias (Acm^{-2})	Zero bias responsivity (A/W)	Extracted i-layer background doping concentration ($\times 10^{15}$ cm^{-3})
A500	500	500	7×10^{-6}	0.27	1.05
A400	400	400	3.5×10^{-5}	0.28	1.65
A300	300	300	1.8×10^{-4}	0.15	20
A300-A	300	300	1.6×10^{-4}	0.28	23
A250	250	250	1.6	0.06	-
A250-A	250	250	0.38	0.24	-
B400	400	500	1.4×10^{-5}	0.25	0.95
B300	300	500	1.7×10^{-5}	0.30	1.25
B250	250	500	4.4×10^{-5}	0.23	1.05

3. Results

I-V measurements from 3-5 devices of each diameter from all wafers showed excellent uniformity. The excellent agreement in reverse dark current densities (normalising current to device area) of devices, indicates dominance of bulk current mechanisms as seen in examples from wafers A500 and A300 in Fig. 1(a). In Fig. 1(b), reverse dark current densities of all wafers plotted against voltage are presented for comparison. Results from set A wafers show significantly increased dark current density as the growth temperature decreases. The dark current density at -1 V changes by more than 6 orders of magnitude, increasing from 7×10^{-6} Acm^{-2} for A500 (grown at 500 °C) to 1.6 Acm^{-2} for A250 (grown at 250 °C). On the other hand, diodes from set B show only a slight degradation of dark currents, within an order magnitude, as the i-layer growth temperature decreases from 400 to 250 °C. Fig. 2(a) plots the dark current densities at a reverse bias of -1 V from all devices to accentuate the impact of the growth temperatures. As can be seen from Figs. 1 and 2(a), the dark current rises rapidly with reduced growth temperature in set A. Comparing diodes grown at 250 °C, the dark current density sees a significant decrease from 1.6 Acm^{-2} to 4.4×10^{-5} Acm^{-2} by changing the growth temperature used for the p and n layers from 250 °C (A250) to 500 °C (B250). Following a postgrowth anneal, diodes from A300-A and A250-A show lower dark current density, as shown in Fig. 1(b) and Fig. 2(a). The improvement in dark current is more pronounced at higher reverse bias as shown in Fig. 1(b).

The zero bias responsivity at 1520 nm wavelength of all wafers are shown in Fig. 2(b). Diodes from set A have responsivity values decreasing from 0.27 to 0.06 A/W as the growth temperature is reduced from 500 to 250 °C. On the other hand, diodes from set B display less variance in responsivity, having values of 0.25, 0.30 and 0.23 A/W for i-layers grown at 400, 300 and 250 °C respectively. Annealing of wafers A300 and A250 gives rise to a pronounced increase in responsivity to 0.28 and 0.24 A/W in wafers A300-A and A250-A, respectively.

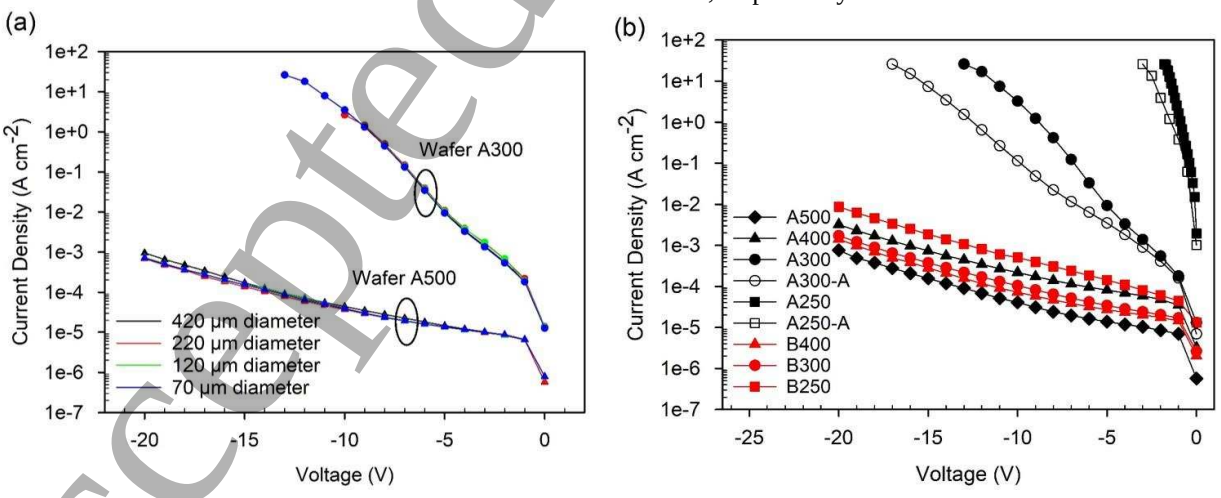

Figure 1. (a) Reverse dark current density versus voltage for wafers A500 and A300. (b) Reverse dark current density versus voltage for all InGaAs wafers.

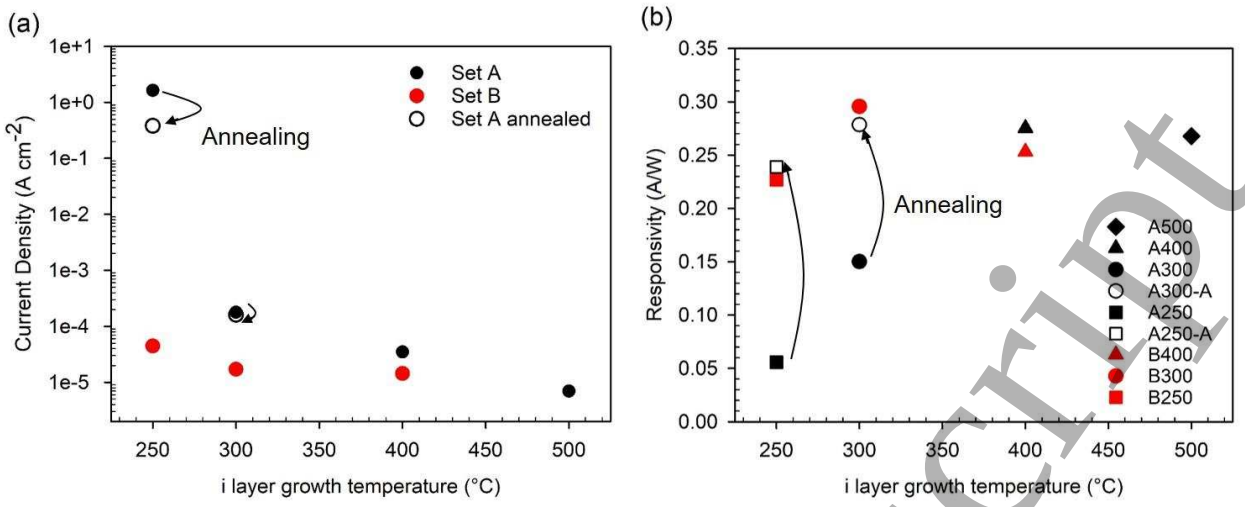

Figure 2. (a) Dark current density at a reverse bias of -1 V and (b) zero bias responsivity at 1520 nm, as a function of growth temperature.

The capacitance data as a function of reverse voltage for all wafers are shown in Fig. 3(a). Excessive dark currents from diodes of A250 and A250-A prevented accurate C-V measurements and, therefore, are not presented in Fig. 3(a). Diodes from wafers A300 and A300-A show higher capacitance values that decrease with reverse bias whereas diodes from other wafers have relatively constant capacitance after a reverse bias of -3 V. The relatively constant capacitance indicates the i-layer is fully depleted in A500, A400, B400, B300 and B250. By modelling the C-V results, i-layer doping concentration between 1 to 2×10^{15} cm^{-3} were obtained for the fully depleted diodes. Doping concentrations that are 20× higher were found in sample A300 and A300-A resulting in the larger capacitance measured. The extracted doping concentration values are shown in Table 1.

The room temperature EL spectra of wafers A500, A300 and A250 are plotted in Fig. 3(b). The EL intensity is significantly reduced in wafers A300 and A250 in contrast to wafer A500, requiring a scaling factor of 50 for comparison. The peak intensity wavelength from the EL spectra shifts from 1667 nm to 1710 nm and the full-width at half maximum increases from 45.7 to 61.1 meV as the growth temperature reduces from 500 to 250 °C.

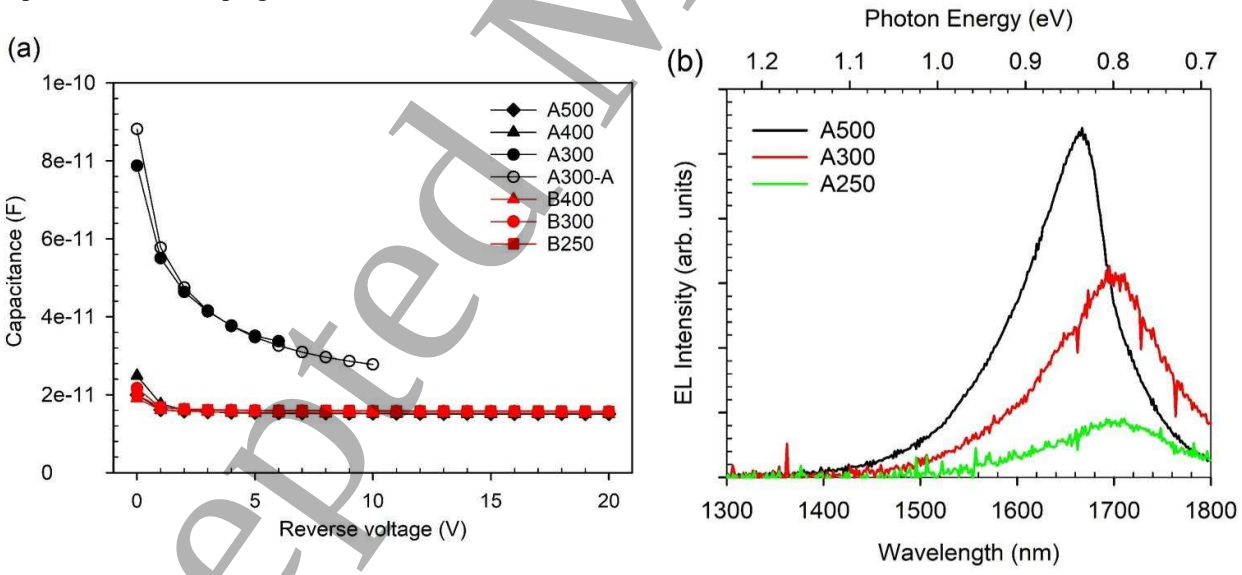

Figure 3. (a) Capacitance against reverse voltage characteristics of InGaAs p-i-n diodes. (b) Room temperature EL spectra of wafers A500, A300 and A250.

4. Discussion

I-V results suggests that in-situ annealing (during the growth of the p-layer at high temperature in set B wafers) minimises the dark current degradation while ex-situ annealing can produce a small reduction in the dark current. The bulk reverse dark current mechanisms at low electric

fields include minority carrier diffusion and generation-recombination (G-R), given by

$$J_{diff} = qn_i^2\left(\frac{D_p}{L_pN_D} + \frac{D_n}{L_nN_A}\right) \quad (1)$$

$$J_{G-R} = \frac{qn_iW}{\tau} \quad (2)$$

where q, n_i and W are the elementary charge, carrier concentration and depletion width respectively while N_D, N_A, D_p, D_n, L_p, L_n and τ are the donor concentration, acceptor concentration, hole diffusion coefficient, electron diffusion coefficient, hole diffusion length, electron diffusion length, and carrier G-R lifetime, respectively.

At higher electric fields band-to-band tunnelling (BBT) and trap-assisted tunnelling (TAT) currents can be significant in narrow bandgap materials. They are given by

$$J_{BBT} = \frac{(2m^*)^{1/2}q^3\xi V}{\mathrm{h}^2E_g^{1/2}}\exp\left(-\frac{a(m^*)^{1/2}E_g^{3/2}}{\mathrm{qh}\xi}\right) \quad (3)$$

$$J_{TAT} = qN_TW\frac{c_pp_1wN_c}{c_pp_1 + wN_c} \quad (4)$$

where the tunnelling rate, wN_c, is given by

$$wN_c = \frac{\pi^2qm^*\xi M^2}{h^3(E_g - E_T)}\exp\left(-\frac{4(2m^*)^{1/2}(E_g - E_T)^{3/2}}{3\mathrm{qh}\xi}\right) \quad (5)$$

where m^*, ξ, V, h, a, and E_g are the electron mass, electric field, applied bias voltage, Planck's constant, tunnelling parameter, and bandgap, respectively. N_T, c_p, p_1, M and E_T are the trap concentration, hole capture coefficient, hole thermal emission rate, matrix element of trap potential energy, and trap energy level, respectively.

Poor crystal quality due to large defect densities (in the form of As point defects) commonly associated with low temperature grown InGaAs [40,41]. This can give rise to reduced minority carrier diffusion length and reduced carrier lifetime. At low bias close to -1 V, the increase in dark current in B400, B300 and B250 can be attributed to an increase in J_{G-R} caused by reduced carrier lifetime as the growth temperature of the i-layer is reduced. When the growth temperature for the p and n layers is also reduced in set A diodes, there is a further increase in J_{diff} arising from the reduced minority carrier diffusion lengths as observed from the higher dark current in A400 compared to B400.

The trends in dark current for A300 and A250 cannot be fully explained using J_{diff} and J_{G-R} which do not increase strongly with voltage. The rapid increase in dark current can be explained qualitatively by fitting the sum of J_{diff}, J_{G-R}, J_{BBT}, and J_{TAT} to the dark current of A250. We extracted an activation energy of 0.06 eV using dark current data at -1 V from 180 to 295 K as shown in Fig. 4(a). We interpret this as E_T to calculate J_{TAT}. In the absence of an accurate value of M, we assume the value used in HgCdTe [42], where

$$wN_c = \frac{6\times10^5\xi}{E_g - E_T}\exp\left(-\frac{1.7\times10^7E_g^{1/2}(E_g - E_T)^{3/2}}{\xi}\right) \quad (6)$$

and use N_T as the fitting parameter to fit the measured dark current as shown in Fig. 4(b). We found that J_{TAT} produces a good fit at bias voltages below -0.4 V, suggesting its dominance at low bias in A250. At higher bias voltages, the more rapid increase in dark current can be explained by the onset of J_{BBT}. A good fit to the measured dark current was obtained by assuming the i-layer of A250 has a doping concentration of 5×10^{17} cm^{-3} (C-V data cannot be extracted accurately due to high dark current). The parameters used for dark current modelling are listed in table II. We noted that growing the p and n layers at high temperature will preserve the low background doping concentration in the i-layers of B250 and B300, such that tunnelling current is not significant.

Our hypothesis of increase in defects that leads to the significant increase in dark current in A300 and A250 is supported by EL data. The EL spectra of wafers grown at low temperatures, A300 and A250, show drastically reduced peak intensity. These results suggest the dominance of non-radiative recombination causing the decrease of EL efficiency, which is most likely due to defect-related recombination which increases as the growth temperature decreases [43]. Similarly, these defects reduce the minority carrier diffusion length that leads to lower responsivity in diodes from set A corroborating the trend observed in the dark current. As light absorption follows an exponential decay function, we expect an illumination wavelength of 1520 nm to be absorbed in the p, i and n layers. Poor crystal quality in all three low temperature grown layers could explain the lower responsivity in set A diodes (due to reduced minority carrier diffusion lengths) as compared to set B diodes. The total photocurrent produced in a p-i-n photodiode is the sum of the drift current due to carriers generated in the depletion region, J_{drift}, and the diffusion current from carriers generated in the p and n layers, J_p and J_n respectively, and are given as

$$J_{drift} = q\Phi_0[1 - \exp(-\alpha W)] \quad (7)$$

$$J_p = qD_n\frac{\partial n_p}{\partial x} = q\Phi_0\frac{\alpha L_n}{1 - \alpha L_n}\exp(-\alpha W) \quad (8)$$

$$J_n = qD_p\frac{\partial p_n}{\partial x} = q\Phi_0\frac{\alpha L_p}{1 - \alpha L_p}\exp(-\alpha W) \quad (9)$$

where Φ_0 and α are the photon flux and absorption coefficient, respectively. It is clear that reduced minority carrier diffusion lengths will reduce the photocurrent. Hence A250 and A300 have lower responsivity values than B250 and B300.

Table II Parameters used for dark current modelling

Parameters	Value	Parameters	Value
Bandgap, E_g	0.75 eV	Carrier lifetime, τ	120×10^{-12} s^{-1}
Electron effective mass, m_e	0.041	Intrinsic carrier concentration, n_i	6.3×10^{17} m^{-3}
Relative permittivity, ε_r	13.9	Trap concentration, N_T	1×10^{21} m^{-3}
p-type acceptor concentration, N_A	5×10^{24} m^{-3}	Hole capture coefficient, c_p	5×10^{-4} m^{3}s^{-1}
Background doping concentration, N_b	5×10^{23} m^{-3}	Hole thermal emission rate, p_1	1.3×10^{13} s^{-1}
Built-in voltage, V_{bi}	0.5 V	Trap energy level, E_T	0.69 eV
Electron diffusion length, L_n	4×10^{-6} m	Tunnelling parameter, α	1.55
Electron diffusion coefficient, D_n	3×10^{-1} m^{2}s^{-1}		

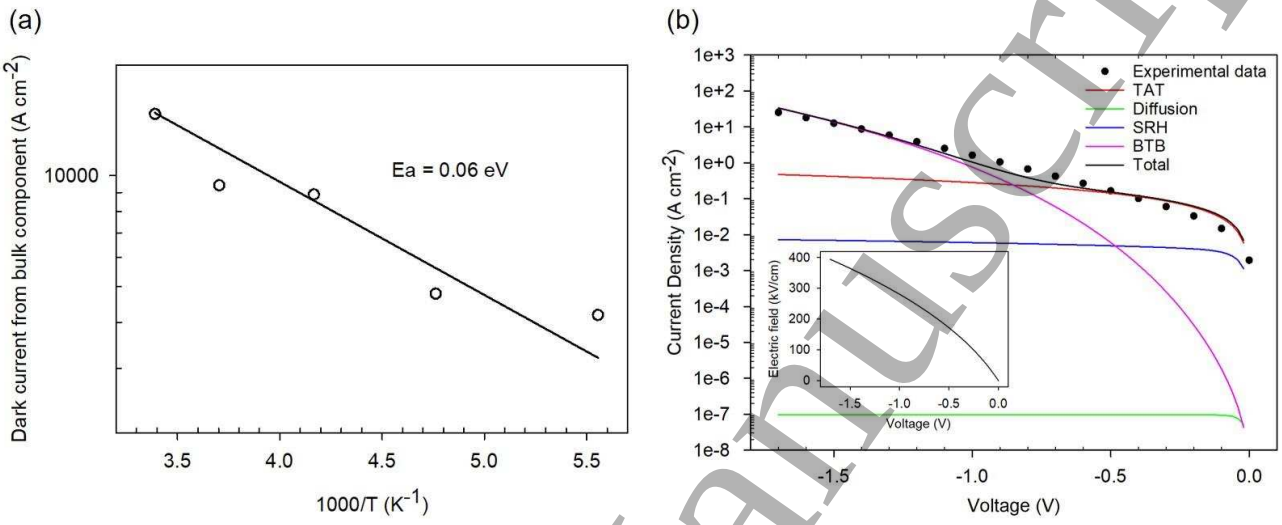

Figure 4. (a) Arrhenius plot of dark current density at -1 V of A250 from 180 to 295 K. (b) Dark current data and modelling of A250. Inset shows the electric field versus applied voltage characteristics for the assumed doping profile.

Devices from the ex-situ annealed wafers, A300-A and A250-A, exhibit improved responsivities over devices from unannealed wafers. From the C-V plots, similar capacitances of A300 and A300-A suggests similar depletion widths in these diodes. Therefore, the increased responsivity in annealed wafers is not caused by changes in J_{drift} but can be attributed to the increased minority carrier diffusion lengths after high temperature annealing. The increase in minority carrier diffusion lengths after annealing also produces a very small reduction in the diffusion dark current as expected from equation (1) and observed in Fig. 2(a). However we found that the diffusion current is several orders of magnitude lower than our measured dark current in A250 as shown in Fig. 4(b). Therefore the small increase of minority carrier diffusion length does not produce notable change in the dark current.

We believe that the increase in the minority carrier diffusion length can be explained as follows. As point defects nucleate to form precipitates following high temperature anneals above 500 °C as observed in low temperature grown InGaAs [40,41]. The electron capture cross sections are reduced in precipitates as compared to antisite defects [44]. Consequently, an increase in minority carrier diffusion length, can be obtained [44] leading to higher responsivities in ex-situ annealed wafers A250-A and A300-A.

For wafers with i-layer grown at 250 and 300 °C, both in-situ and ex-situ annealing increase responsivity to levels comparable to diodes grown at conventional temperature (A500 diodes). However, postgrowth ex-situ annealing does not offer significant improvement to the dark current. This is consistent with reports for GaInNAs(Sb) laser diodes, where in-situ annealing was found to result in superior recovery in performance over ex-situ annealing [45]. Therefore we believe a high temperature cap layer growth is needed to improve device performance in materials that necessitate low growth temperatures.

5. Conclusion

Experimental data of InGaAs p-i-n photodiodes grown at different temperatures has been presented. Decreasing the growth temperature from 500 to 250 °C in all p, i and n layers leads to 6 orders of magnitude increase in dark current at -1 V and 4.5 times lower responsivity at 0 V. The poor diode properties are attributed to defects originating from excess As incorporation in low temperature growth wafers as reported in literature and supported by results from C-V and EL measurements. For wafers grown at 250 and 300 °C, postgrowth ex-situ annealing at 595 °C improves the diode responsivity but fails to produce a significant improvement in dark current. We found that raising the growth temperature of

the p layer to 500 °C during growth (in-situ annealing) after the i-layer was grown at a lower temperature provides much better responsivity and dark current values. A 5 orders magnitude drop in dark current and 3.8 times increase in responsivity is observed when a high growth temperature of 500 °C is employed for the p and n layers in diodes with i-layer grown at 250 °C. Growing the p and n layers at high temperature was also found to maintain the background doping concentration in the i-layer, hence minimising the tunnelling current.

These results suggest that poor device performance due to reduced minority carrier diffusion lengths and increase in the background doping concentration caused by low growth temperature can be avoided by growing the p and n layers at a high temperature.

Acknowledgements

This work was funded by the UK Engineering and Physical Sciences Research Council (EPSRC) grant EP/N020715/1 and EP/N021037/1. The authors would like to acknowledge wafer growth from the EPSRC National Epitaxy Facility, Sheffield, UK.

References

[1] Hansen M P and Douglas S M 2008 Thermosense XXX **6939** 69390I
[2] Zhang Y, Gu Y, Zhu C, Hao G, Li A Z and Liu T 2006 Infrared Phys. Technol. **47(3)** 257
[3] Ong D S, Ng J S, Goh Y L, Tan C H, Zhang S and David J P 2010 IEEE Trans. Electron Devices **58** 486
[4] Hoang A M, Chen G, Haddadi A, Abdollahi P S and Razeghi M 2012 Appl. Phy. Lett. **100** 211101
[5] Zhou X, Meng X, Krysa A B, Willmott J R, Ng J S and Tan C H 2015 IEEE Sens. J. **15** 5555
[6] Zhang Y G, Gu Y, Wang K, Li A Z and Li C 2008 Semicond. Sci. Technol. **23** 125029
[7] Rothman J et al 2012 J. Electron. Mater. **41** 2928
[8] The Minamata Convention on Mercury www.mercuryconvention.org/
[9] Gu Y, Zhang Y G, Chen X Y, Ma Y J, Xi S P, Du B and Li H 2016 Appl. Phys. Lett. **108** 032102
[10] Du B, Gu Y, Zhang Y G, Chen X Y, Ma Y J, Shi Y H and Zhang J 2018 Chin. Phys. Lett. **35** 078501
[11] Fukano H, Mitsuhara M and Kondo Y 2008 IEEE LEOS 294
[12] Nagarajan R et al 2010 IEEE J. Sel. Top. Quantum Electron. **16** 1113
[13] Kondow M, Kazuhisa U, Atsuko N, Takeshi K, Seiji W and Yoshiaki Y 1996 Jpn. J. Appl. Phys. **35** 1273
[14] Oe K and Okamoto H 1998 Jpn. J. Appl. Phys. **37** L1283
[15] Weyers M, Sato M and Ando H 1992 Jpn. J. Appl. Phys. **31** 853
[16] Geisz J F, Friedman D J, Olson J M, Kurtz S R and Keyes B M 1998 J. Cryst. Growth **195** 401
[17] Balkan N, Erol A, Sarcan F, Al-Ghuraibawi L F and Nordin M S 2015 Superlattice Microst. **86** 467
[18] Tixier S, Adamcyk M, Tiedje T, Francoeur S, Mascarenhas A, Wei P and Schiettekatte F 2003 Appl. Phys. Lett. **82** 2245
[19] Marko I P and Sweeney S J 2017 IEEE J. Sel. Top. Quantum Electron. **23** 1
[20] Feng G, Yoshimoto M, Oe K, Chayahara A and Horino Y 2005 Jpn. J. Appl. Phys. **44** L1161
[21] Sandall I, Bastiman F, White B, Richards R, Mendes D, David J P, Tan C H 2014 Appl. Phys. Lett. **104** 171109
[22] Tan S L et al 2010 Proc. SPIE **7726**
[23] Pavulescu E M, Wagner J, Komsa H P, Rantal T T, Dumitrescu M and Pessa M 2005 J. Appl. Phys. **98** 083524
[24] Reason M, McKay H A, Ye W, Hanson S, Goldman R S and Rotberg V 2004 Appl. Phys. Lett. **85** 1692
[25] Serries D, Geppert T, Ganser P, Maier M, Köhler K, Herres N and Wagner J 2002 Appl. Phys. Lett. **80** 2448
[26] Wei J, Lin W, Thomson K J and Forrest S R 2001 IEEE Photon. Technol. Lett. **13** 352
[27] Yoshikawa M, Miura K, Iguchi Y and Kawamura Y 2009 J. Cryst. Growth **311** 1745
[28] Yoshimoto M, Murata S, Chayahara A, Horino Y, Saraie J and Oe K 2003 Jpn. J. Appl. Phys. **42** L1235
[29] Richards R D, Bastiman F, Hunter C J, Mendes D F, Mohmad A R, Roberts J S and David J P 2014 J. Cryst. Growth **390** 120
[30] Rockett T B, Richards R D, Gu Y, Harun F, Liu Y, Zhou Z and David J P 2017 J. Cryst. Growth **477** 139
[31] Zhong Y, Dongmo P B, Petropoulos J P and Zide J M 2012 Appl. Phys. Lett. **100** 112110
[32] Stall R A, Wunder R J, Swaminathan V and Cox H M 1985 Appl. Phys. Lett. **47** 518
[33] Cheng K Y, Cho A Y, Wagner W R and Bonner W A 1981 J. Appl. Phys. **52** 1015
[34] Gregory I S, Baker C, Tribe W R, Evans M J, Beere H E, Linfield E H, Davies A G and Missous M 2003 Appl. Phys. Lett. **83** 4199
[35] Claverie A, Yu K M, Swider W, Liliental-Weber Z, O'keefe M, Kilaas R, Pamulapati J and Bhattacharya P K 1992 Appl. Phys. Lett. **60** 989
[36] Khirouni K, Alaya S, Nagle J and Bourgoin J C 1998 Semicond. Sci. Technol. **13** 1031
[37] Künzel H, Böttcher J, Gibis R and Urmann G 1992 Appl. Phys. Lett. **61** 1347
[38] Metzger R A, Brown A S, McCray L G and Henige J A 1993 J. Vac. Sci. Technol. B **11** 798
[39] Sharpe M K et al 2019 J. Appl. Phys. **126** 125706
[40] Ibbetson J P, Speck J S, Gossard A C and Mishra U K 1993 Appl. Phys. Lett. **62** 2209
[41] Grandidier B, Chen H, Feenstra R M, McInturff D T, Juodawlkis P W and Ralph S E 1999 Appl. Phys. Lett. **74** 1439
[42] Nemirovsky Y, Fastow R, Meyassed M and Unikovsky A 1991 AIP Conf. Proc. **235** 1829
[43] Marko I P et al 2014 J. Phys. D **47** 345103
[44] Baker C, Gregory I S, Tribe W R, Bradley I V, Evans M J, Linfield E H and Missous M 2004 Appl. Phys. Lett. **85** 4965
[45] Zhao H, Xu Y Q, Ni H Q, Zhang S Y, Han Q, Du Y, Yang X H, Wu R H and Niu Z C 2005 Semicond. Sci. Technol. **21** 279